

Beyond Independent Labels: Schwartz-Geometry Decoding for Human Value Detection

Víctor Yeste^{1,2,*} and Paolo Rosso^{1,3}

¹PRHLT Research Center, Universitat Politècnica de València, Spain

²School of Science, Engineering and Design, Universidad Europea de Valencia, Spain

³Valencian Graduate School and Research Network of Artificial Intelligence (ValgrAI)

*Corresponding author: vicyesmo@upv.es

Abstract

Human value detection is commonly formulated as sentence-level multi-label classification over the 19 refined Schwartz values, typically predicted as independent labels. Schwartz theory, however, describes them as a circular motivational continuum, in which adjacent values are compatible and opposing values are in tension. We ask whether this structure can be operationalized as an explicit output-space geometry and used as a soft bias rather than a hard constraint. On a DeBERTa-v3-base classifier, we compare two ways of injecting it: training-time geometry-aware objectives and a post-hoc Schwartz-aware energy decoder that scores whole label sets jointly. Across five seeds, training-time geometry gives only limited gains—no larger for the true continuum than for a random ordering—whereas the decoder makes label sets more coherent with the continuum—on theory-aware coherence metrics we introduce—at no cost to Macro-F1 or Micro-F1 (held fixed by its selection rule). The gain is specific to the true Schwartz ordering: it does not appear for a random permutation or an empirical co-occurrence graph through the identical decoder. A bounded Qwen2.5-72B-Instruct diagnostic shows that supplying the continuum at inference shifts behavior but does not match supervised structured prediction. Theory-aware decoding thus offers a lightweight, controllable way to make value detection faithful to its label space.

supports work across NLP and computational social science. The task is commonly posed as sentence-level multi-label classification: given a sentence, predict which refined human values it expresses (Kiesel et al., 2023; Mirzakhmedova et al., 2024). The dominant modeling approach treats the values as independent labels. This is convenient but theoretically incomplete: the refined Schwartz theory defines the values not as independent categories but as a circular motivational continuum, in which neighboring values are compatible and values on opposite arcs are in tension (Schwartz et al., 2012; Schwartz, 2017; Schwartz and Ciecuch, 2022).

We ask whether this theory can be made operational in value detection without overconstraining it. The goal is not a hard rule that opposite values can never co-occur—real texts express conflict, compromise, and trade-offs (Schwartz et al., 2017; Skimina et al., 2018)—but a soft inductive bias: can a model preserve predictive performance while producing label sets that are more coherent with the Schwartz continuum? The question is timely. Recent work on the same task shows that strong flat encoders are hard to beat (Ma et al., 2023; Molazadeh Oskuee et al., 2023; Yeste and Rosso, 2026b), while hard architectural uses of the theory, such as presence gates or higher-order hierarchies, can introduce recall bottlenecks or error propagation (Yeste and Rosso, 2026a). It is also sharpened by instruction-tuned LLMs, which can be prompted with the theory directly (Sun, 2024; Zhu et al., 2025), raising the question of whether supervised structure is still needed.

We encode the 19 refined values as a circular output-space geometry—an angular position per value and a circular distance matrix—and use it in two ways: a training-time penalty and a post-

1 Introduction

Human values underlie moral, social, political, and cultural language, and detecting them in text

hoc structured decoder over a DeBERTa-v3-base classifier. Across five seeds, training-time geometry yields only limited, non-theory-specific gains, whereas the Schwartz decoder improves theory-aware coherence at no cost to F1, and only for the true continuum—not a random permutation or an empirical co-occurrence graph. A bounded 72B LLM diagnostic shows that prompting the theory shifts behavior but does not match the supervised decoder.

We make four contributions: (i) we formulate sentence-level detection of the 19 refined Schwartz human values as a circular output-space geometry, with a family of theory-aware coherence metrics derived from it; (ii) we compare training-time geometry-aware objectives with a post-hoc Schwartz-aware energy decoder on the same classifier, finding that only the decoder yields label sets more coherent with the continuum; (iii) we isolate the role of the true geometry through direct random and empirical control comparisons with paired significance tests; and (iv) we add a bounded LLM diagnostic testing whether prompted theory can replace supervised structured prediction. By *coherence* we mean a concrete, measurable property of the predicted label set: fewer false positives on the far side of the circle and confusions concentrated among nearby values rather than opposing ones (operationalized in Section 5). Together, the results support theory-aware decoding as a lightweight, controllable way to make value detection more faithful to the psychological structure of its label space.

2 Related Work

Human value detection. Identifying the human values behind arguments was introduced by Kiesel et al. (2022) and scaled into the ValueEval shared task and an extended benchmark family (Kiesel et al., 2023; Mirzakhmedova et al., 2024). Rooted in argument mining (Lawrence and Reed, 2019), the setting also supports downstream argumentation and deliberation analysis (Plenz et al., 2024). More broadly, detecting values and morality in text is a central goal of computational social science, as in work grounded in Moral Foundations Theory, its annotated corpora, and its links to language models (Graham et al., 2009; Hoover et al., 2020; Zangari et al., 2025). These moral and value signals also support downstream tasks such as hate-speech detection and identifying violent rad-

icalization (Vargas et al., 2026; Yin et al., 2026). Beyond argument mining, recent work measures the (often subjective) expression of basic Schwartz human values directly in social-media posts (Epstein et al., 2026), underscoring that value attributions are annotator- and context-dependent. Strong shared-task systems rely on transformer encoders—often DeBERTa—together with class-imbalance handling, threshold tuning, and ensembling (Ma et al., 2023; Molazadeh Oskuee et al., 2023; Kandru et al., 2023; Tsunokake et al., 2023; Aydin et al., 2024). Recent work on sentence-level detection of the refined values further reports that such direct encoders and calibration (Guo et al., 2017) are strong, while presence gates and higher-order hierarchies can introduce recall bottlenecks or error propagation (Yeste and Rosso, 2026a,b). Across this line, however, the values are typically predicted as independent labels or organized by a hard hierarchy, and the motivational geometry of the label space is left implicit. We instead make that geometry an explicit, soft component of the output space.

Schwartz values and motivational structure.

The refined Schwartz theory, building on the original circular value model (Schwartz, 1992), arranges 19 basic values on a circular motivational continuum in which adjacent values share compatible goals and opposing values express tension (Schwartz et al., 2012; Schwartz, 2017)—a structure with broad cross-cultural psychometric support and predictive links to behavior (Schwartz and Cieciuch, 2022; Cieciuch and Schwartz, 2013; Bardi and Schwartz, 2003). This makes the label space theoretically structured rather than arbitrary. We use the continuum as an inductive bias and evaluation lens, not as a hard constraint on what a text may express, since real arguments can voice value tensions and trade-offs (Schwartz et al., 2017; Skimina et al., 2018). Circular, continuous structure of this kind is not unique to values: affective constructs are organized as a circumplex (Russell, 1980) or an emotion wheel (Plutchik, 1980), and such structured label spaces are increasingly modeled in NLP (Demszky et al., 2020), which motivates treating the continuum as an output-space geometry rather than as unordered classes.

Structured multi-label prediction. Multi-label learning has long modeled label dependence

(Tsoumakas and Katakis, 2007)—through classifier chains (Read et al., 2011), neural sequence-generation decoders (Yang et al., 2018), label-correlation and embedding methods, and graph-based structures (Zhang and Zhou, 2014; Huang et al., 2024; Tarekegn et al., 2024). A complementary line casts prediction as structured inference or energy minimization over label configurations, from conditional random fields and collective classification (Lafferty et al., 2001; Ghamrawi and McCallum, 2005) to structured prediction energy networks (Belanger and McCallum, 2016); our decoder shares this view but fixes the pairwise term from theory rather than learning it. In these approaches the dependencies are typically learned from training co-occurrence or label semantics. Our work keeps a strong local classifier and adjusts only the final prediction with a structured decoding objective; the distinguishing feature is that the structure is derived from a psychological theory and tested directly against random and empirical control geometries.

LLMs for value classification. Prompted large language models are increasingly applied to value and moral classification—comparing prompting with fine-tuning, value identification and annotation (Sun, 2024; Zhu et al., 2025; Milkova and Rudnev, 2026; Yeste and Rosso, 2026c; de la Cruz Fernández et al., 2025), probing Schwartz value priorities (Segerer, 2025), assessing moral abilities against human labels (Bulla et al., 2025), analyzing values in real-world interactions (Huang et al., 2025), and ensembling detectors (Rodrigues et al., 2024). Rather than benchmarking many models, we include one bounded diagnostic asking whether supplying the continuum at inference time can match incorporating it through supervised training and decoding.

3 Task and Schwartz Geometry

3.1 Task and Data

We study sentence-level human value detection as multi-label classification over the 19 refined Schwartz values. Given a sentence x , a model predicts a binary vector $y \in \{0, 1\}^{19}$, where $y_k = 1$ indicates that value v_k is expressed in x . We use the Touché24-ValueEval data family (Kiesel et al., 2023; Mirzakhmedova et al., 2024), segmented and annotated at the sentence level following recent work on refined-value detection (Yeste and

	Train	Dev	Test
Documents	1,603	523	522
Sentences	44,758	14,904	14,569
≥ 1 value	23,062	7,600	7,402
(% of split)	51.5	51.0	50.8
> 1 value	2,640	876	901
Values / positive sent.	1.13	1.13	1.14

Table 1: Dataset statistics. Splits are partitioned by document, with no `Text-ID` shared across splits. The label space is the 19 refined Schwartz values in all splits.

Rosso, 2026b).¹

Each value carries two stance annotations, *attained* and *constrained*. Because our object of study is the geometry of value *presence* rather than stance, we collapse the two stances into a single presence indicator: $y_k = 1$ iff value v_k is annotated as attained or constrained, and 0 otherwise. This yields a standard binary multi-label target compatible with sigmoid outputs and threshold-based decoding.

We use the official train/validation/test partition, split by document (`Text-ID`) so no document is shared across splits and sentence-level overlap cannot inflate test performance (Table 1). About half of all sentences express at least one value (50.8–51.5% across splits), and value-positive sentences are predominantly single-label (≈ 1.1 values each); multi-value sentences are a non-negligible minority (e.g., 901 test sentences). Per-label support is strongly imbalanced, from *Humility* (0.24%) to *Security: societal* (8.6%; full distribution in Appendix B). All hyperparameters and thresholds are selected on validation only; the test split is used once.

3.2 Circular Value Geometry

The refined Schwartz theory arranges the 19 values on a circular motivational continuum: adjacent values share compatible motivational goals, whereas values on opposite arcs express conflicting motivations (Schwartz et al., 2012; Schwartz, 2017; Schwartz and Cieciuch, 2022)—a compatibility-and-conflict structure with confirmatory empirical support (Schwartz and Boehnke, 2004). The continuum spans four higher-order

¹The corpus is distributed under a restricted Data Usage Agreement via Zenodo (The ValuesML Team, *Touché24-ValueEval*, 2024, <https://doi.org/10.5281/zenodo.13283288>).

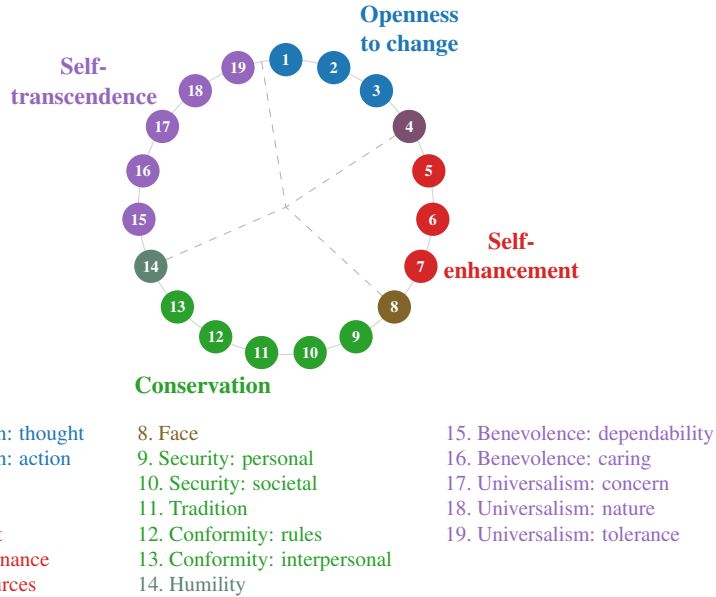


Figure 1: The refined Schwartz value continuum used as the output-space geometry. The 19 values are placed in canonical order around the circle and colored by higher-order region; Hedonism (4), Face (8) and Humility (14) bridge adjacent regions. Adjacent values are motivationally compatible, while values on opposite arcs are in tension. The four dashed radial lines mark the two bipolar dimensions (openness to change vs. conservation; self-enhancement vs. self-transcendence).

regions—*openness to change*, *self-enhancement*, *conservation*, and *self-transcendence*—with Hedonism, Face, and Humility bridging adjacent regions (Figure 1). We fix this canonical order as the backbone of an output-space geometry.

We place value v_k at angle $\theta_k = 2\pi k/19$, $k \in \{0, \dots, 18\}$, on the unit circle, with embedding $e_k = (\cos \theta_k, \sin \theta_k)$. The normalized circular distance between two values is the shorter arc between their positions,

$$d(v_i, v_j) = \frac{\min(|\theta_i - \theta_j|, 2\pi - |\theta_i - \theta_j|)}{\pi} \quad (1)$$

$$= \frac{2}{19} \min(|i - j|, 19 - |i - j|),$$

so that $d = 0$ for identical values and d approaches 1 for diametrically opposed values. Because 19 is odd there is no exact antipode, and the maximum attainable distance is $18/19 \approx 0.95$. The resulting 19×19 matrix D is the single quantity from which every geometry-aware term in the paper is derived.

From D we read off two relations used later by the objectives, decoder, and metrics: **neighbor compatibility**—pairs within two steps on the circle ($1 \leq \min(|i - j|, 19 - |i - j|) \leq 2$), expected to co-occur more plausibly—and **opposite tension**—pairs with $d > 0.75$ (at least eight steps apart), treated as conflicting and requiring stronger evidence to be predicted jointly.

We stress that this geometry is a soft inductive bias, not a hard constraint: the refined structure has broad cross-cultural psychometric support (Schwartz and Cieciuch, 2022), but real texts can express tension or compromise, so opposing values are penalized rather than forbidden.

To test whether any benefit is specific to the *true* Schwartz structure rather than to structure in general, we compare D against two controls built with the same machinery. A **random circular geometry** applies Equation 1 to a seeded random permutation of the 19 values, preserving the circular form but destroying the theory-derived ordering. An **empirical co-occurrence geometry** uses distances $1 - \text{Jaccard}(i, j)$ from training-split label co-occurrence (Huang et al., 2024), capturing data-derived dependency rather than motivational theory.

4 Methods

All supervised systems share one architecture: a DeBERTa-v3-base encoder (He et al., 2023) with a linear head mapping the pooled sentence representation to 19 logits z , with $p = \sigma(z)$. They differ only in (i) the training objective and (ii) an optional post-hoc decoding step; the encoder, optimization, data protocol, and seeds are held fixed (Section 5), so differences reflect the objective or

decoder, not model capacity. We use the distance matrix D and its neighbor and opposite relations throughout. Our main method is the post-hoc decoder of Section 4.3; training-time geometry (Section 4.2) is an alternative way to inject the same structure. We use three adjectives with distinct scopes: *theory-aware* (faithful to Schwartz theory by any mechanism), *geometry-aware* (any method using the distance matrix D , including the controls), and *Schwartz-aware* (specifically the true continuum).

4.1 Independent Supervised Baselines

The primary baseline trains the classifier with binary cross-entropy (BCE) over the 19 labels, treating them as independent. As an imbalance-aware baseline we also train with asymmetric loss (ASL) (Ridnik et al., 2021), which adds two terms to BCE: it clips and down-weights easy negative labels through a focal-style modulation, focusing learning on positives and hard negatives. This is motivated by the strong label imbalance in the data (Appendix B). At inference, both baselines convert probabilities to labels with per-label thresholds τ tuned on validation, $\hat{y}_k = \mathbb{1}[p_k \geq \tau_k]$.

4.2 Geometry-Aware Training

Training-time variants inject the geometry directly into the objective, leaving inference unchanged. **GeoLoss** adds to a base loss $\mathcal{L}_{\text{base}} \in \{\text{BCE}, \text{ASL}\}$ a distance-weighted penalty $\lambda \mathbb{E}_x [\sum_{i,j} y_i D_{ij} p_j / \sum_i y_i]$, so that probability mass placed on values far from the gold set on the circle is penalized in proportion to its circular distance. **GeoSmooth** instead replaces the binary targets with geometry-smoothed soft targets $\tilde{y}_j = \max_i y_i \exp(-D_{ij}^2/\tau)$ (clamped to retain the original positives) before applying the base loss, giving nearby values a small amount of soft supervision; GeoSmooth is thus a distance-aware form of label smoothing (Szegedy et al., 2016; Pereyra et al., 2017; Müller et al., 2019; Díaz and Marathe, 2019). Both λ and τ are tuned on validation.

The same machinery defines our structure controls by swapping the matrix D : **random GeoLoss** uses a seeded random circular permutation, and **empirical structure** uses the co-occurrence distances of Section 3. If any structure helps, the random control should help too; if data-derived dependency suffices, the empirical control should match the true geometry.

4.3 Schwartz-Aware Energy Decoder

Our main method keeps the trained classifier fixed and replaces independent thresholding with a structured decoder applied to its probabilities. Intuitively, it picks the label set that keeps the labels the classifier already supports, rewards co-selecting compatible neighbors, and penalizes co-selecting opposing values—a structured alternative to thresholding each label in isolation. For a sentence x , the decoder selects the label set that maximizes a structured score—equivalently, the negative of an energy in the sense of energy-based models (LeCun et al., 2006)—that combines classifier evidence with the Schwartz geometry,

$$\hat{y} = \arg \max_{y \in \mathcal{Y}(x)} \left[\sum_k y_k u_k(x) + \frac{1}{2} \sum_{i \neq j} y_i y_j W_{ij} - \gamma (\sum_k y_k - 1)_+ \right]. \quad (2)$$

The unary term $u_k(x) = \sigma^{-1}(p_k(x)) - \sigma^{-1}(\tau_k)$ is the classifier’s log-odds margin over the validation-tuned threshold, so it is positive exactly when $p_k \geq \tau_k$. The pairwise weights $W_{ij} = \alpha N_{ij} - \beta O_{ij}$ combine the neighbor-compatibility matrix N (a soft weight that is largest for immediate neighbors and decays to zero beyond two steps) and the opposite mask O (one for pairs with $D_{ij} > 0.75$): with $\alpha, \beta \geq 0$, co-selecting neighbors is rewarded and co-selecting opposing values is penalized. The final term is a cardinality penalty ($\gamma \geq 0$, applied beyond the first label) that discourages over-large sets. When $\alpha = \beta = \gamma = 0$ the maximizer reduces exactly to BCE thresholding, so the decoder is a strict generalization of the baseline. To keep the maximization exact and cheap, $\mathcal{Y}(x)$ is restricted to a small pool of high-scoring labels (threshold-positive, high-probability, and top-ranked), capped at a few candidates and a few decoded labels per sentence; exact cut-offs are in Section 5.

The weights (α, β, γ) are tuned on validation under a Pareto criterion: among settings that retain Macro-F1 within a small tolerance of the best validation Macro-F1, we select the one that minimizes a validation geometry cost (a label-set coherence measure defined in Section 5). This is, by construction, the reason the decoder improves theory-aware coherence while preserving F1: F1 preservation is enforced by the Pareto constraint

rather than discovered empirically. The test set is decoded once with the selected weights. The identical decoder is run with the Schwartz, random, and empirical geometries (N , O derived from each), providing the same controls as in training. Like other structured multi-label methods it adjusts a strong local classifier’s output, but its pairwise structure is theory-derived rather than learned from data (Read et al., 2011; Zhang and Zhou, 2014).

4.4 LLM Diagnostic

To test whether the theory can instead be supplied at inference time to a large language model, we include a bounded diagnostic with Qwen2.5-72B-Instruct (Qwen et al., 2025) under two prompts. Both state the task, the attained/constrained-to-presence convention, and the 19 value definitions, and require a strict JSON label list drawn only from the allowed values; they differ only in that the *continuum* prompt additionally describes the circular ordering and the expectation that nearby values are compatible while opposing values usually conflict. Decoding is deterministic (temperature 0). Outputs are parsed against the exact allowed label set, and we record an invalid-output rate for responses that cannot be parsed without repair. This isolates theory injected through prompting from theory injected through training or decoding; full prompts are in Appendix E.

5 Experimental Setup

Data and protocol. All systems use the sentence-level splits of Section 3 with the document-level partition. Hyperparameters and thresholds are selected on validation; the test split is evaluated once. Each supervised configuration is run with five seeds (42, 7, 1701, 11, 1984), and we report mean and standard deviation over seeds.

Backbone and optimization. All supervised systems fine-tune `deberta-v3-base` with AdamW (Loshchilov and Hutter, 2019). Base hyperparameters are selected once on validation by grid search over learning rate ($\{6, 7, 8, 9, 10\} \times 10^{-6}$) and weight decay ($\{0.10, \dots, 0.20\}$), yielding 10^{-5} and 0.15; effective batch size (16), sequence length (1024 tokens), and gradient clipping (1.0) are fixed. We train up to 30 epochs with early stopping (patience 3) and tune per-label thresholds τ on validation by sweeping $[0, 1]$ in steps of 0.01 to maximize each label’s F1.

Hyperparameter selection. Objective- and decoder-specific hyperparameters are likewise selected on validation. For ASL we search $\gamma_{\text{neg}} \in \{2, 3, 4, 5\}$ and $\text{clip} \in \{0, 0.03, 0.05, 0.1\}$ with $\gamma_{\text{pos}} = 0$; for GeoLoss $\lambda \in \{0.01, 0.05, 0.1, 0.2\}$; and for GeoSmooth $\tau \in \{0.1, 0.2, 0.5, 1.0\}$. The energy decoder uses fixed component magnitudes (neighbor $\alpha = 0.1$, opposite $\beta = 0.2$, cardinality $\gamma = 0.02$) and a two-step neighbor window. The candidate pool for each sentence is the union of the threshold-positive labels, labels with probability above half the tuned threshold or above 0.01, and the eight highest-probability labels; it is capped at eight candidates and the decoded set at five labels. Validation selection under the Pareto rule of Section 4.3 (retain validation Macro-F1 within 99% of thresholding, then minimize the validation geometry cost) determines which components are active; in our final runs it keeps the neighbor and opposite terms but sets the cardinality term to $\gamma = 0$.

Metrics. We report three standard metrics—Macro-F1, Micro-F1, and threshold-free Macro-AUPRC—together with a family of theory-aware metrics that we introduce for this label space (in the spirit of distance-weighted and ordinal error measures such as the earth mover’s distance (Rubner et al., 2000; Hou et al., 2016) and of hierarchical-classification evaluation (Kosmopoulos et al., 2015)), derived from the circular geometry. Because probabilities and discrete label sets call for different theory-aware measures, the supervised models and the decoder are scored with different ones (hence the differing theory-aware columns in Tables 2 and 3). For supervised models, which emit probabilities, we report the *expected circular error*: the gold-normalized, distance-weighted probability mass placed away from the gold values (lower is better), i.e. the quantity penalized by GeoLoss. For the structured decoder, which emits label sets, we report label-set metrics: the *opposite-error rate*, the share of false-positive labels that are opposite ($D > 0.75$) to every gold value (lower is better); the *neighbor-error rate*, the share falling within two steps of a gold value (near-miss errors); and the *confusion-distance correlation* between label-pair circular distance and confusion frequency. The *decoder geometry cost* sums these three—two rates in $[0, 1]$ and a correlation in $[-1, 1]$, equally weighted—

so a lower value is more coherent. All three are corpus-level quantities computed once per configuration, so selection picks a single global (α, β, γ) under the Macro-F1 constraint, not a per-sentence rule. As the composite is dimensionally heterogeneous, we report its components separately (Section 6.2) and treat the Schwartz-vs-control contrast, not the absolute cost, as the primary evidence.

Significance testing. For decoder and LLM comparisons we use paired, sample-level bootstrap tests (Dror et al., 2018) (2,000 resamples) on the shared test set, reporting two-sided p -values at the 0.05 level. This includes the direct Schwartz-vs-control tests on decoder geometry cost. For the supervised systems (Table 2), which we summarize by five per-seed scores, we instead use a paired seed-level bootstrap against the BCE baseline over the shared seeds. Full deltas and p -values for both families of tests are tabulated in Appendix C.

LLM diagnostic. The diagnostic runs Qwen2.5-72B-Instruct (4-bit quantization) with deterministic decoding (temperature 0, at most 128 new tokens) under the two prompts of Appendix E. Responses are parsed against the exact 19-label set; unparseable responses are counted in the invalid-output rate and contribute no labels.

Reproducibility. To preserve anonymity, we describe software and release plans in general terms. Configurations, training and decoding scripts, tuned thresholds, and model predictions will be released as a project artifact after review.²

6 Results

6.1 Training-Time Geometry Gives Limited Gains

Table 2 reports the supervised systems. BCE is a strong, stable baseline (Macro-F1 0.2934).³ Asymmetric loss does not help here: it is slightly weaker on every standard metric and much less

²Code, configurations, tuned thresholds, and model predictions are available at <https://github.com/VictorMYeste/schwartz-geometry-value-detection>.

³For reference, prior work on the same sentence-level task reports a comparable direct-classifier Macro-F1 (≈ 0.281 , deberta-base, fixed 0.5 threshold) (Yeste and Rosso, 2026b); the setups are not strictly comparable (we use deberta-v3-base with tuned per-label thresholds), so we read this only as a check that our baseline is competitive.

stable across seeds (Macro-F1 0.2833 ± 0.0193 ; circular error 0.374 ± 0.181). The three GeoLoss-based variants (empirical, random, and Schwartz) all fall within one standard deviation of BCE on the standard metrics, and the Schwartz GeoLoss gain over BCE is not significant (paired bootstrap, $p = 0.19$ for Macro-F1). They reduce expected circular error slightly (to 0.127–0.131 from 0.134), but the random control reduces it as much as the true geometry, so the effect is not specific to the Schwartz structure. GeoSmooth is the clear exception: in this formulation the soft targets destabilize training and collapse performance (Macro-F1 0.1651, significantly below BCE, $p < 0.001$). These conclusions are unchanged when the objectives are paired with the imbalance-aware ASL base instead of BCE: all variants remain below their BCE counterparts and GeoSmooth again collapses (Appendix A). Training-time geometry thus yields no consistent or theory-specific gain, motivating the post-hoc decoder.

6.2 Schwartz Decoding Improves Label-Set Coherence

The decoder is the main positive result. Applied to the BCE classifier (Table 3), the Schwartz decoder leaves predictive performance essentially unchanged—Macro-F1 $0.2934 \rightarrow 0.2943$, Micro-F1 $0.3425 \rightarrow 0.3430$, neither significant—while lowering the *decoder geometry cost* (the corpus-level sum of opposite-error rate, neighbor-error rate, and confusion–distance correlation; Section 5) from 0.5634 to 0.5480. Two caveats keep this honest: the F1 preservation is guaranteed by the Pareto selection rule (Section 4.3), not discovered, and the reduction against the decoder’s own thresholding baseline is a sanity check—the substantive evidence is the controlled comparison of Section 6.3. The reduction is driven by the opposite-error rate ($0.5092 \rightarrow 0.5072$) and the confusion–distance correlation ($-0.137 \rightarrow -0.154$); the neighbor-error rate rises slightly ($0.191 \rightarrow 0.195$; Section 7).

The edits are small and surgical: the decoder changes only $2.45\% \pm 0.26\%$ of test sentences (≈ 357 of 14,569), so the average set size barely moves ($0.804 \rightarrow 0.803$ labels per sentence; total predicted labels $11,718 \rightarrow 11,699$, $\approx 0.16\%$). With the validation-selected cardinality weight at $\gamma = 0$, the coherence gain is not an artifact of predicting more or fewer labels. The claim is thus de-

Method	Macro-F1 \uparrow	Micro-F1 \uparrow	Macro-AUPRC \uparrow	Circ. err. \downarrow
BCE	0.2934 \pm 0.0037	0.3425 \pm 0.0060	0.2353 \pm 0.0067	0.1342 \pm 0.0138
ASL	0.2833 \pm 0.0193	0.3306 \pm 0.0219	0.2235 \pm 0.0240	0.3735 \pm 0.1812
Empirical structure	0.2945 \pm 0.0053	0.3401 \pm 0.0048	0.2356 \pm 0.0074	0.1269 \pm 0.0101
Random GeoLoss	0.2949 \pm 0.0058	0.3439 \pm 0.0085	0.2353 \pm 0.0059	0.1273 \pm 0.0105
Schwartz GeoLoss	0.2958 \pm 0.0051	0.3421 \pm 0.0086	0.2356 \pm 0.0051	0.1305 \pm 0.0096
Schwartz GeoSmooth	0.1651 \pm 0.0063	0.1656 \pm 0.0105	0.1182 \pm 0.0053	0.6988 \pm 0.0758

Table 2: Supervised test results (mean \pm std, five seeds). \uparrow/\downarrow = higher/lower is better. BCE and the three GeoLoss variants coincide within seed noise on standard metrics; GeoSmooth collapses. Best per column **bold**.

liberately narrow: more theory-coherent label sets at no measurable cost to F1.

6.3 The True Schwartz Geometry Matters

The decoder rows of Table 3 already show that the random and empirical geometries barely move the geometry cost; the cleanest test, however, is a direct paired comparison. Relative to the controls run through the identical decoder, the Schwartz geometry lowers the decoder geometry cost by 0.0145 (vs. random; 95% bootstrap CI [0.0074, 0.0231]) and 0.0148 (vs. empirical; CI [0.0074, 0.0231]), significant in all five seeds ($p < 0.001$; the per-seed tests share the same direction, so we report them without multiple-comparison correction), whereas the corresponding Macro-F1 and Micro-F1 differences are negligible (≤ 0.001) and significant in none. Matching the label count, the circular form, or the empirical co-occurrence structure is therefore not sufficient: the coherence gain comes from the Schwartz ordering itself.

6.4 Prompted LLMs Do Not Replace Supervised Structured Prediction

Table 4 compares the two prompted Qwen2.5-72B-Instruct configurations with the supervised systems. Both prompts trail the supervised models by a wide, significant margin on standard metrics: Qwen reaches Macro-F1 0.2430/0.2396 and Micro-F1 0.2730/0.2643 (definitions/continuum) against 0.2934/0.3425 for BCE thresholding (5/5 seeds, $p < 0.001$ on both). This is not a formatting artifact—the invalid-output rate is below 0.2% under both prompts. Adding the Schwartz continuum to the prompt does shift geometry-aware behavior, lowering the geometry cost from 0.5757 to 0.5633 ($p = 0.01$) and roughly doubling the average number of predicted labels (1.07 \rightarrow 1.50), though it slightly lowers F1. The continuum-prompted cost (0.5633) essentially matches untuned BCE thresholding (0.5634) but not the de-

coder’s (0.5480): prompting reaches the baseline’s coherence, not the decoder’s. The comparison is intentionally asymmetric—zero-shot prompting against a classifier fine-tuned on $\approx 45k$ in-domain sentences—so it is a bounded probe of whether prompting suffices, and the supervised win is expected. Prompted theory thus moves behavior in the expected direction without matching supervised structured prediction.

7 Analysis and Discussion

A consistent pattern across our experiments is that the Schwartz geometry helps as a post-hoc decoder but not when injected into the training loss. We read this as a division of labor. The supervised encoder already learns strong local evidence for each value, so a geometry penalty on the loss mostly perturbs an already-good objective—and for GeoSmooth the cross-value soft targets, in this particular formulation, are aggressive enough to destabilize training and collapse performance. Independent thresholding, by contrast, discards label dependencies at the final decision step, which is exactly where the decoder operates: it reconciles per-label evidence into a coherent set without altering the learned representations. The same view explains why the training-time circular-error gains are small and not theory-specific—a random ordering helps as much as the true one (Table 2)—while the decoder’s neighbor and opposite terms act on the discrete label set, where the ordering does matter.

The controlled comparison isolates this effect: only the true Schwartz ordering lowers the decoder geometry cost, whereas a random circular permutation and an empirical co-occurrence graph do not. Qualitatively, the decoder edits predictions in the two ways the theory anticipates. It suppresses opposite-side false positives—for a sentence whose gold label is *Power: dom-*

Decoder	Macro-F1 \uparrow	Micro-F1 \uparrow	Opp. err. \downarrow	Geom. cost \downarrow
BCE thresholding	0.2934 \pm 0.0037	0.3425 \pm 0.0060	0.5092 \pm 0.0096	0.5634 \pm 0.0120
+ empirical decoder	0.2935 \pm 0.0037	0.3428 \pm 0.0063	0.5100 \pm 0.0092	0.5628 \pm 0.0119
+ random decoder	0.2935 \pm 0.0038	0.3429 \pm 0.0062	0.5099 \pm 0.0091	0.5625 \pm 0.0115
+ Schwartz decoder	0.2943 \pm 0.0034	0.3430 \pm 0.0063	0.5072 \pm 0.0098	0.5480 \pm 0.0130

Table 3: Structured decoder on the BCE classifier (mean \pm std, five seeds), run under each geometry; Opp. err. and Geom. cost lower-is-better. F1 is preserved everywhere, but only the Schwartz geometry materially lowers geometry cost. Best **bold**.

System	Macro-F1 \uparrow	Micro-F1 \uparrow	Geom. cost \downarrow	Inval. % \downarrow
Qwen definitions	0.2430	0.2730	0.5757	0.08
Qwen continuum	0.2396	0.2643	0.5633	0.14
BCE thresholding	0.2934	0.3425	0.5634	—
BCE + Schwartz decoder	0.2943	0.3430	0.5480	—

Table 4: LLM diagnostic vs. supervised systems (LLM: single deterministic run; supervised: five-seed mean). “Inval. %”: share of responses not parsable without repair. The continuum prompt lowers geometry cost but not below the decoder, and both prompts trail supervised F1. Best per column **bold**.

inance, thresholding also fires *Benevolence: dependability* and *Universalism: concern*, two self-transcendence values on the far arc, which the decoder removes—and it completes near-neighbor sets, as when thresholding emits only *Power: dominance* for a gold *Power: resources* and the decoder adds the adjacent true value. Both edits raise sample-level F1 while reducing distant activations; Appendix D tabulates these and further examples.

The neighbor-error rate needs care, as it enters the minimized cost yet the decoder completes neighbor sets. It counts only *false-positive* neighbors (within two steps of a gold value): completing a correct neighbor removes a near-miss and lowers it, while adding a wrong one raises it. Because the decoder adds some unsupported neighbors, the corpus rate rises slightly (0.191 \rightarrow 0.195) and the net gain comes from the opposite-error and confusion-distance terms. This is why we minimize the composite, not any single term, and read the controlled contrast as decisive.

We are deliberate about what improves. The decoder targets the structured label set, not per-label calibration, so its gains surface in label-set coherence rather than probability-mass metrics or large F1 jumps; Macro-F1 and Micro-F1 stay within seed noise. The contribution is thus a more theory-consistent decision layer at no measurable cost to accuracy, not a new state of the art—by design, since the Schwartz circle is a soft bias and real texts express genuine value conflict that a coher-

ence objective should discourage only when unsupported, not forbid.

This soft, post-hoc use of the theory aligns with findings that hard architectural encodings of Schwartz structure are brittle on this task (Yeste and Rosso, 2026a,b): our decoder leaves the flat classifier intact and adds structure only as a final, tunable adjustment. The LLM diagnostic points the same way from the other side: prompting the continuum steers Qwen2.5-72B-Instruct toward more geometry-coherent behavior but trades away F1 and stays well below the supervised systems. The controllable supervised decoder is thus the more reliable way to make predictions respect the value space’s structure.

8 Limitations, Ethics, and Conclusion

Limitations. Our scope is deliberately narrow: one dataset family (Touché24-ValueEval), English, sentence-level inputs, and one backbone (DeBERTa-v3-base); we do not test other languages, domains, longer contexts, or larger encoders. The improvement we measure is coherence, not accuracy—the decoder lowers theory-aware costs while leaving Macro-F1 and Micro-F1 within seed noise—so its value is more consistent, interpretable label sets, not higher standard scores. The decoder geometry cost is a composite we define rather than an established benchmark, and the circular operationalization (equal angular spacing, canonical order, opposite threshold $D > 0.75$, two-step neighbor window) is one reason-

able choice among several; a mis-specified geometry could in principle suppress genuine value conflict, which the soft penalty discourages but does not forbid. Because the decoder reranks candidate sets from the classifier’s own probabilities, it cannot recover values the base model never surfaces and inherits any miscalibration of those probabilities and thresholds. Finally, the LLM diagnostic uses a single model and two prompts under deterministic decoding; it is a bounded probe whose numbers may shift with the model, prompt, or decoding.

Ethics. Human value detection can support research on social, political, and moral language, but it can also be misused to profile individuals or infer sensitive beliefs. Sentence-level attributions are uncertain and culturally variable, and our systems should be read as tools for aggregate analysis and annotation support, not as verdicts about individual speakers. Theory-aware decoding improves structural consistency with the Schwartz taxonomy; it does not remove annotation noise, ambiguity, or cross-cultural differences in how values are expressed, and it should not be treated as evidence that a person holds a value.

Conclusion. Human value detectors need not treat the refined Schwartz values as independent labels. Injecting the circular structure into the training loss is informative but not decisive—GeoLoss matches the baseline within noise and GeoSmooth degrades it—whereas a post-hoc Schwartz-aware decoder, holding Macro-F1 and Micro-F1 fixed by its selection rule, makes label sets measurably more coherent with the continuum, and only when the geometry is the true one (random and empirical controls do not; significant in all five seeds). Prompting an LLM with value definitions or the continuum shifts behavior but does not close the gap to supervised structured prediction. What sets this apart from prior work is where and how the theory enters: unlike hard hierarchies or architectural gates on this task, which can bottleneck recall (Yeste and Rosso, 2026a,b), and unlike structured decoders that learn label dependencies from data co-occurrence (Read et al., 2011; Zhang and Zhou, 2014), we fix the pairwise structure from theory, keep it a soft bias rather than a hard constraint, and apply it post-hoc to an untouched classifier, then test it directly against random and empirical control geometries; to mea-

sure this faithfulness we also introduce a family of theory-aware coherence metrics. More broadly, a psychological theory is most useful here as a soft, controllable output-space bias applied at decoding time. We conjecture, but do not test, that the recipe could extend to other label spaces with known scientific structure (e.g. circumplex or wheel models of emotion); that transfer is left to future work.

Acknowledgments

The authors used Claude Opus 4.8 and Claude Fable 5 for language polishing, structural editing, and assistance in drafting prose from author-provided notes, tables, and verified experimental results. The authors reviewed and edited all generated text and are responsible for all claims, analyses, and citations. These models were also used to assist with code organization and result-extraction scripts; all code and outputs were manually inspected by the authors.

References

- Aisha Nur Aydin, Shaden Shaar, and Claire Cardie. 2024. Edward said at touché: Human value detection using transformers and upsampling. In *CLEF 2024 Working Notes*.
- Anat Bardi and Shalom H. Schwartz. 2003. [Values and behavior: Strength and structure of relations](#). *Personality and Social Psychology Bulletin*, 29(10):1207–1220.
- David Belanger and Andrew McCallum. 2016. Structured prediction energy networks. In *Proceedings of the 33rd International Conference on Machine Learning (ICML)*, pages 983–992.
- Luana Bulla, Stefano De Giorgis, Misael Mongiovì, and Aldo Gangemi. 2025. [Large language models meet moral values: A comprehensive assessment of moral abilities](#). *Computers in Human Behavior Reports*, 17:100609.
- Jan Ciecuch and Shalom H. Schwartz. 2013. [Applying the refined values theory to past data: What can researchers gain?](#) *Journal of Cross-Cultural Psychology*, 44(8):1215–1234.
- Eduardo de la Cruz Fernández, Marcelo Karanik, and Sascha Ossowski. 2025. [Value Lens: Using large language models to understand human values](#). In *European Conference on Artificial*

- Intelligence (ECAI)*, volume 413 of *Frontiers in Artificial Intelligence and Applications*, pages 5175–5178.
- Dorottya Demszky, Dana Movshovitz-Attias, Jeongwoo Ko, Alan Cowen, Gaurav Nemade, and Sujith Ravi. 2020. [GoEmotions: A dataset of fine-grained emotions](#). In *Proceedings of the 58th Annual Meeting of the Association for Computational Linguistics (ACL)*, pages 4040–4054.
- Raúl Díaz and Amit Marathe. 2019. Soft labels for ordinal regression. In *Proceedings of the IEEE/CVF Conference on Computer Vision and Pattern Recognition (CVPR)*, pages 4738–4747.
- Rotem Dror, Gili Baumer, Segev Shlomov, and Roi Reichart. 2018. [The hitchhiker’s guide to testing statistical significance in natural language processing](#). In *Proceedings of the 56th Annual Meeting of the Association for Computational Linguistics (Volume 1: Long Papers)*, pages 1383–1392, Melbourne, Australia. Association for Computational Linguistics.
- Ziv Epstein, Farnaz Jahanbakhsh, Tiziano Piccardi, Isabel Gallegos, Dora Zhao, Johan Ugander, and Michael S. Bernstein. 2026. [Whose values? measuring the \(subjective\) expression of basic human values in social media posts](#). *Proceedings of the International AAAI Conference on Web and Social Media*, 20(1):738–759.
- Nadia Ghamrawi and Andrew McCallum. 2005. [Collective multi-label classification](#). In *Proceedings of the 14th ACM International Conference on Information and Knowledge Management (CIKM)*, pages 195–200.
- Jesse Graham, Jonathan Haidt, and Brian A. Nosek. 2009. [Liberals and conservatives rely on different sets of moral foundations](#). *Journal of Personality and Social Psychology*, 96(5):1029–1046.
- Chuan Guo, Geoff Pleiss, Yu Sun, and Kilian Q. Weinberger. 2017. On calibration of modern neural networks. In *Proceedings of the 34th International Conference on Machine Learning (ICML)*, pages 1321–1330.
- Pengcheng He, Jianfeng Gao, and Weizhu Chen. 2023. [DeBERTaV3: Improving DeBERTa using ELECTRA-style pre-training with gradient-disentangled embedding sharing](#). In *The Eleventh International Conference on Learning Representations (ICLR)*.
- Joe Hoover, Gwenyth Portillo-Wightman, Leigh Yeh, Shreya Havaldar, Aida Mostafazadeh Davani, Ying Lin, Brendan Kennedy, Mohammad Atari, Zahra Kamel, Madelyn Mendlen, Gabriela Moreno, Christina Park, Tingyee E. Chang, Jenna Chin, Christian Leong, Jun Yen Leung, Arineh Mirinjian, and Morteza Dehghani. 2020. [Moral Foundations Twitter Corpus: A collection of 35k tweets annotated for moral sentiment](#). *Social Psychological and Personality Science*, 11(8):1057–1071.
- Le Hou, Chen-Ping Yu, and Dimitris Samaras. 2016. [Squared earth mover’s distance-based loss for training deep neural networks](#). *arXiv preprint arXiv:1611.05916*.
- Saffron Huang, Esin Durmus, Miles McCain, Kunal Handa, Alex Tamkin, Jerry Hong, Michael Stern, Arushi Somani, Xiuruo Zhang, and Deep Ganguli. 2025. [Values in the wild: Discovering and analyzing values in real-world language model interactions](#). *arXiv preprint arXiv:2504.15236*.
- Shan Huang, Wei Hu, Baoyu Lu, Qian Fan, Xiaoning Xu, Xiaolin Zhou, and Hao Yan. 2024. [Application of label correlation in multi-label classification: A survey](#). *Applied Sciences*, 14(19):9034.
- Pavan Kandru, Bhavyajeet Singh, Ankita Maity, Kancharla Aditya Hari, and Vasudeva Varma. 2023. [Tenzin-gyatso at SemEval-2023 task 4: Identifying human values behind arguments using DeBERTa](#). In *Proceedings of the 17th International Workshop on Semantic Evaluation (SemEval-2023)*. Association for Computational Linguistics.
- Johannes Kiesel, Milad Alshomary, Nicolas Handke, Xiaoni Cai, Henning Wachsmuth, and Benno Stein. 2022. [Identifying the human values behind arguments](#). In *Proceedings of the 60th Annual Meeting of the Association for Computational Linguistics (Volume 1: Long Papers)*, pages 4459–4471, Dublin, Ireland. Association for Computational Linguistics.

- Johannes Kiesel, Milad Alshomary, Nailia Mirzakhmedova, Maximilian Heinrich, Nicolas Handke, Henning Wachsmuth, and Benno Stein. 2023. [SemEval-2023 Task 4: ValueEval: Identification of human values behind arguments](#). In *Proceedings of the 17th International Workshop on Semantic Evaluation (SemEval-2023)*, pages 2287–2304, Toronto, Canada. Association for Computational Linguistics.
- Aris Kosmopoulos, Ioannis Partalas, Eric Gaussier, Georgios Paliouras, and Ion Androutsopoulos. 2015. [Evaluation measures for hierarchical classification: a unified view and novel approaches](#). *Data Mining and Knowledge Discovery*, 29(3):820–865.
- John D. Lafferty, Andrew McCallum, and Fernando C. N. Pereira. 2001. Conditional random fields: Probabilistic models for segmenting and labeling sequence data. In *Proceedings of the Eighteenth International Conference on Machine Learning (ICML)*, pages 282–289.
- John Lawrence and Chris Reed. 2019. [Argument mining: A survey](#). *Computational Linguistics*, 45(4):765–818.
- Yann LeCun, Sumit Chopra, Raia Hadsell, Marc’Aurelio Ranzato, and Fu Jie Huang. 2006. A tutorial on energy-based learning. In *Predicting Structured Data*. MIT Press.
- Ilya Loshchilov and Frank Hutter. 2019. [Decoupled weight decay regularization](#). In *International Conference on Learning Representations (ICLR)*.
- Long Ma, Zeye Sun, Jiawei Jiang, and Xuan Li. 2023. [PAI at SemEval-2023 task 4: A general multi-label classification system with class-balanced loss function and ensemble module](#). In *Proceedings of the 17th International Workshop on Semantic Evaluation (SemEval-2023)*. Association for Computational Linguistics.
- Maria Milkova and Maksim Rudnev. 2026. Measuring human value expression in social media texts: Calibrated LLM annotation and encoder transfer. *arXiv preprint arXiv:2606.11018*.
- Nailia Mirzakhmedova, Johannes Kiesel, Milad Alshomary, Maximilian Heinrich, Nicolas Handke, Xiaoni Cai, Valentin Barriere, Henning Wachsmuth, and Benno Stein. 2024. [The Touché23-ValueEval dataset for identifying human values behind arguments](#). In *Proceedings of the 2024 Joint International Conference on Computational Linguistics, Language Resources and Evaluation (LREC-COLING 2024)*, pages 16121–16134, Torino, Italy.
- Milad Molazadeh Oskuee, Mostafa Rahgouy, Hamed Babaei Giglou, and Cheryl D. Seals. 2023. [TM Scanlon at SemEval-2023 task 4: Leveraging pretrained language models for human value argument mining with contrastive learning](#). In *Proceedings of the 17th International Workshop on Semantic Evaluation (SemEval-2023)*. Association for Computational Linguistics.
- Rafael Müller, Simon Kornblith, and Geoffrey Hinton. 2019. When does label smoothing help? In *Advances in Neural Information Processing Systems (NeurIPS)*, volume 32.
- Gabriel Pereyra, George Tucker, Jan Chorowski, Łukasz Kaiser, and Geoffrey E. Hinton. 2017. [Regularizing neural networks by penalizing confident output distributions](#). *arXiv preprint arXiv:1701.06548*.
- Moritz Plenz, Philipp Heinisch, Anette Frank, and Philipp Cimiano. 2024. [Pakt: Perspectivized argumentation knowledge graph and tool for deliberation analysis](#). In *Robust Argumentation Machines*, pages 89–107, Cham. Springer Nature Switzerland.
- Robert Plutchik. 1980. [A general psychoevolutionary theory of emotion](#). In Robert Plutchik and Henry Kellerman, editors, *Emotion: Theory, Research, and Experience*, volume 1, pages 3–33. Academic Press.
- Qwen, An Yang, Baosong Yang, Beichen Zhang, Binyuan Hui, Bo Zheng, Bowen Yu, Chengyuan Li, Dayiheng Liu, Fei Huang, Haoran Wei, Huan Lin, Jian Yang, Jianhong Tu, Jianwei Zhang, Jianxin Yang, Jiayi Yang, Jingren Zhou, Junyang Lin, Kai Dang, Keming Lu, Keqin Bao, Kexin Yang, Le Yu, Mei Li, Mingfeng Xue, Pei Zhang, Qin Zhu, Rui Men, Runji Lin, Tianhao Li, Tianyi Tang, Tingyu Xia, Xingzhang Ren, Xuancheng Ren, Yang Fan, Yang Su, Yichang Zhang, Yu Wan, Yuqiong Liu, Zeyu Cui, Zhenru Zhang, and Zihan Qiu.

2025. Qwen2.5 technical report. *arXiv preprint arXiv:2412.15115*.
- Jesse Read, Bernhard Pfahringer, Geoff Holmes, and Eibe Frank. 2011. [Classifier chains for multi-label classification](#). *Machine Learning*, 85(3):333–359.
- Tal Ridnik, Emanuel Ben-Baruch, Nadav Zamir, Asaf Noy, Itamar Friedman, Matan Protter, and Lihi Zelnik-Manor. 2021. Asymmetric loss for multi-label classification. In *Proceedings of the IEEE/CVF International Conference on Computer Vision (ICCV)*, pages 82–91.
- Diego Dimer Rodrigues, Mariana Recamonde-Mendoza, and Viviane P. Moreira. 2024. [Beyond single models: Leveraging LLM ensembles for human value detection in text](#). In *Proceedings of the 15th Brazilian Symposium in Information and Human Language Technology (STIL)*, pages 372–381. Sociedade Brasileira de Computação.
- Yossi Rubner, Carlo Tomasi, and Leonidas J. Guibas. 2000. [The earth mover’s distance as a metric for image retrieval](#). *International Journal of Computer Vision*, 40(2):99–121.
- James A. Russell. 1980. [A circumplex model of affect](#). *Journal of Personality and Social Psychology*, 39(6):1161–1178.
- Shalom H. Schwartz. 1992. [Universals in the content and structure of values: Theoretical advances and empirical tests in 20 countries](#). In Mark P. Zanna, editor, *Advances in Experimental Social Psychology*, volume 25, pages 1–65. Academic Press.
- Shalom H. Schwartz. 2017. [The refined theory of basic values](#). In Sonia Roccas and Lilach Sagiv, editors, *Values and Behavior: Taking a Cross Cultural Perspective*, pages 51–72. Springer.
- Shalom H. Schwartz and Klaus Boehnke. 2004. [Evaluating the structure of human values with confirmatory factor analysis](#). *Journal of Research in Personality*, 38(3):230–255.
- Shalom H. Schwartz and Jan Cieciuch. 2022. [Measuring the refined theory of individual values in 49 cultural groups: Psychometrics of the revised Portrait Value Questionnaire](#). *Assessment*, 29(5):1005–1019.
- Shalom H. Schwartz, Jan Cieciuch, Michele Vecchione, Eldad Davidov, Ronald Fischer, Constanze Beierlein, Alice Ramos, Markku Verkasalo, Jan-Erik Lönnqvist, Kursad Demirutku, Ozlem Dirilen-Gumus, and Mark Konty. 2012. [Refining the theory of basic individual values](#). *Journal of Personality and Social Psychology*, 103(4):663–688.
- Shalom H. Schwartz, Jan Cieciuch, Michele Vecchione, Claudio Torres, Ozlem Dirilen-Gumus, and Tania Butenko. 2017. [Value tradeoffs and behavior in five countries: Validating 19 refined values](#). *European Journal of Social Psychology*, 47(3):241–258.
- Robin Segerer. 2025. Cultural value alignment in large language models: A prompt-based analysis of Schwartz values in Gemini, ChatGPT, and DeepSeek. *arXiv preprint arXiv:2505.17112*.
- Ewa Skimina, Jan Cieciuch, Shalom H. Schwartz, Eldad Davidov, and René Algesheimer. 2018. [Testing the circular structure and importance hierarchy of value states in real-time behaviors](#). *Journal of Research in Personality*, 74:42–49.
- Pingwei Sun. 2024. [Fine-tuning vs prompting, can language models understand human values?](#) *arXiv preprint arXiv:2403.09720*.
- Christian Szegedy, Vincent Vanhoucke, Sergey Ioffe, Jon Shlens, and Zbigniew Wojna. 2016. Rethinking the Inception architecture for computer vision. In *Proceedings of the IEEE Conference on Computer Vision and Pattern Recognition (CVPR)*, pages 2818–2826.
- Adane Nega Tarekegn, Mohib Ullah, and Faouzi Alaya Cheikh. 2024. Deep learning for multi-label learning: A comprehensive survey. *arXiv preprint arXiv:2401.16549*.
- Grigorios Tsoumakos and Ioannis Katakis. 2007. [Multi-label classification: An overview](#). *International Journal of Data Warehousing and Mining*, 3(3):1–13.
- Masaya Tsunokake, Atsuki Yamaguchi, Yuta Ko-reeda, Hiroaki Ozaki, and Yasuhiro Sogawa. 2023. [Hitachi at SemEval-2023 task 4: Exploring various task formulations reveals the importance of description texts on human values](#). In *Proceedings of the 17th International Workshop*

on *Semantic Evaluation (SemEval-2023)*. Association for Computational Linguistics.

Francielle Vargas, Jackson Trager, Diego Alves, Surendrabikram Thapa, Matteo Guida, Berk Atil, Daryna Dementieva, Andrew Smart, and Ameeta Agrawal. 2026. Self-explaining hate speech detection with moral rationales. *arXiv preprint arXiv:2601.03481*.

Pengcheng Yang, Xu Sun, Wei Li, Shuming Ma, Wei Wu, and Houfeng Wang. 2018. **SGM: Sequence generation model for multi-label classification**. In *Proceedings of the 27th International Conference on Computational Linguistics (COLING)*, pages 3915–3926.

Victor Yeste and Paolo Rosso. 2026a. **Do Schwartz higher-order values help sentence-level human value detection? a study of hierarchical gating and calibration**. *arXiv preprint arXiv:2602.00913*.

Victor Yeste and Paolo Rosso. 2026b. **Human values in a single sentence: Moral presence, hierarchies, and transformer ensembles on the Schwartz continuum**. *arXiv preprint arXiv:2601.14172*.

Victor Yeste and Paolo Rosso. 2026c. **More context, larger models, or moral knowledge? a systematic study of Schwartz value detection in political texts**. *arXiv preprint arXiv:2605.22641*.

Ming Yin, Miao Wan, Zihao Lin, and Jijiao Jiang. 2026. **Moralization-aware identity fusion for detecting violent radicalization in social media**. *Information Processing & Management*, 63(2, Part A):104413.

Lorenzo Zangari, Candida Maria Greco, Davide Picca, and Andrea Tagarelli. 2025. **A survey on moral foundation theory and pre-trained language models: current advances and challenges**. *AI & SOCIETY*, 40(6):4973–4998.

Min-Ling Zhang and Zhi-Hua Zhou. 2014. **A review on multi-label learning algorithms**. *IEEE Transactions on Knowledge and Data Engineering*, 26(8):1819–1837.

Wenhao Zhu, Yuhang Xie, Guojie Song, and Xin Zhang. 2025. **Eavit: efficient and accurate human value identification from text data via**

llms. In *Proceedings of the Thirty-Fourth International Joint Conference on Artificial Intelligence, IJCAI '25*.

A Geometry-Aware Training on the ASL Base

Table 5 repeats the geometry-aware objectives on the imbalance-aware ASL base. The picture is unchanged: every variant trails the BCE-based systems (Table 2), the GeoLoss variants do not even beat the plain ASL baseline, and Schwartz GeoSmooth again collapses, more severely than under BCE. Training-time geometry is thus not decisive regardless of base loss, and the GeoSmooth instability is not specific to BCE.

B Per-Label Distribution

Table 6 reports per-value support over the full corpus, in canonical Schwartz order. Support spans roughly two orders of magnitude (*Humility* to *Security: societal*), motivating the imbalance-aware baseline (Section 4) and validation-tuned per-label thresholds.

C Full Significance Tests

Table 7 reports the paired seed-level bootstrap (Section 5) behind Table 2: the mean test-set delta of each supervised variant against BCE over the five shared seeds, with two-sided p -values. No GeoLoss variant differs significantly from BCE on a standard metric; only the empirical control significantly reduces circular error, and GeoSmooth is significantly worse on every metric. Table 8 reports the paired sample-level bootstrap behind Section 6.3: per-seed tests of the Schwartz decoder against each control geometry on the shared test set. The geometry-cost reduction is significant in every seed against both controls, while the F1 differences are significant in none.

D Qualitative Decoder Edits

Table 9 lists representative test sentences whose label sets the Schwartz decoder edits, covering the two edit types discussed in Section 7: completing a nearby true value and removing opposite-side false positives (the third and fourth rows are the two examples described there). Each row shows the gold labels, the thresholding output, the decoded output, and the sentence-level F1 change.

Method (ASL base)	Macro-F1 \uparrow	Micro-F1 \uparrow	Macro-AUPRC \uparrow	Circ. err. \downarrow
ASL (baseline)	0.2833 ± 0.0193	0.3306 ± 0.0219	0.2235 ± 0.0240	0.3735 ± 0.1812
+ empirical structure	0.2879 ± 0.0048	0.3322 ± 0.0067	0.2306 ± 0.0042	0.1750 ± 0.0167
+ random GeoLoss	0.2703 ± 0.0040	0.3189 ± 0.0028	0.2136 ± 0.0044	0.1299 ± 0.0058
+ Schwartz GeoLoss	0.2763 ± 0.0054	0.3235 ± 0.0090	0.2197 ± 0.0050	0.1273 ± 0.0057
+ Schwartz GeoSmooth	0.2081 ± 0.0146	0.2383 ± 0.0173	0.1513 ± 0.0107	0.8776 ± 0.1307

Table 5: Geometry-aware training on the ASL base (test, mean \pm std over five seeds). All variants trail the BCE-based systems of Table 2; the GeoLoss variants do not beat the plain ASL baseline, and GeoSmooth collapses. F1 and AUPRC are higher-is-better; circular error is lower-is-better. Best per column in **bold**.

Value	Region	Support (%)
Self-direction: thought	O	1.24
Self-direction: action	O	3.52
Stimulation	O	2.64
Hedonism	O/SE	0.82
Achievement	SE	6.38
Power: dominance	SE	4.53
Power: resources	SE	5.07
Face	SE/C	1.83
Security: personal	C	2.07
Security: societal	C	8.64
Tradition	C	1.36
Conformity: rules	C	6.19
Conformity: interpersonal	C	1.35
Humility	C/ST	0.24
Benevolence: dependability	ST	1.95
Benevolence: caring	ST	2.28
Universalism: concern	ST	4.89
Universalism: nature	ST	2.15
Universalism: tolerance	ST	1.04

Table 6: Per-label support as a percentage of all corpus sentences ($N = 74,231$), in canonical Schwartz order. Regions: O = openness to change, SE = self-enhancement, C = conservation, ST = self-transcendence; Hedonism (O/SE) and Face (SE/C) bridge two regions.

E LLM Diagnostic Prompts

Both prompts are built from the fixed template below, reproduced verbatim from the experiment code; the only per-sentence variation is the target sentence. The *continuum* prompt inserts the marked block between the definitions and the output rules; the *definitions* prompt omits it. Definitions follow canonical Schwartz order. Italic parenthetical annotations are ours, not part of the prompt.

You are a sentence-level classifier for human values.

Task: identify which of the 19 refined Schwartz values are expressed in the

target sentence.

The labels collapse attained and constrained cases into value presence: predict a label if the sentence expresses that value in either form.

Allowed labels and definitions:

- Self-direction: thought: freedom to cultivate one’s own ideas and abilities.

- Self-direction: action: freedom to determine one’s own actions.

- Stimulation: excitement, novelty, and change.

- Hedonism: pleasure and sensuous gratification.

- Achievement: success according to social standards.

- Power: dominance: power through exercising control over people.

- Power: resources: power through control of material and social resources.

- Face: maintaining one’s public image and avoiding humiliation.

- Security: personal: safety in one’s immediate environment.

- Security: societal: safety and stability in the wider society.

- Tradition: maintaining and preserving cultural, family, or religious traditions.

- Conformity: rules: compliance with rules, laws, and formal obligations.

- Conformity: interpersonal: avoidance of upsetting or harming other people.

- Humility: recognising one’s insignificance in the larger scheme of things.

- Benevolence: dependability: being a reliable and trustworthy member of the in-group.

- Benevolence: caring: devotion to the welfare of in-group members.

- Universalism: concern: commitment to equality, justice, and protection for all people.

- Universalism: nature: preservation of the natural environment.

- Universalism: tolerance: acceptance and understanding of those who are

Method (vs. BCE)	Macro-F1		Micro-F1		Macro-AUPRC		Circ. err.	
	Δ	p	Δ	p	Δ	p	Δ	p
ASL	-0.0101	0.170	-0.0119	0.193	-0.0118	0.170	+0.2393	< 0.001
Empirical structure	+0.0012	0.721	-0.0024	0.186	+0.0002	0.878	-0.0073	0.008
Random GeoLoss	+0.0015	0.488	+0.0014	0.640	-0.0001	0.775	-0.0069	0.097
Schwartz GeoLoss	+0.0025	0.191	-0.0004	0.809	+0.0003	0.882	-0.0037	0.164
Schwartz GeoSmooth	-0.1282	< 0.001	-0.1769	< 0.001	-0.1172	< 0.001	+0.5646	< 0.001

Table 7: Paired seed-level bootstrap for the supervised systems of Table 2: mean test delta vs. BCE over the five shared seeds (2,000 resamples; two-sided p). Positive Δ favors the variant on F1/AUPRC; negative Δ favors it on circular error. Significant p (< 0.05) in bold.

Control	Metric	Δ	Sig.	Max p
Random	Geom. cost	-0.0145	5/5	< 0.001
Random	Opp. err.	-0.0027	4/5	0.96
Random	Macro-F1	+0.0008	0/5	0.83
Random	Micro-F1	+0.0002	0/5	0.77
Empirical	Geom. cost	-0.0148	5/5	< 0.001
Empirical	Opp. err.	-0.0028	4/5	0.96
Empirical	Macro-F1	+0.0008	0/5	0.79
Empirical	Micro-F1	+0.0002	0/5	0.80

Table 8: Paired sample-level bootstrap for the decoder-control comparison of Section 6.3, run per seed (2,000 resamples). Δ = Schwartz – control, averaged over seeds (negative is better for cost and error); “Sig.” counts seeds with two-sided $p < 0.05$; “Max p ” is the largest per-seed p -value, in bold when significant (< 0.05). The 95% confidence intervals for the geometry-cost deltas appear in Section 6.3.

different from oneself.

Schwartz-continuum structure:

(continuum prompt only)

- The refined values are arranged around this motivational circle:

Self-direction: thought ->

Self-direction: action -> Stimulation

-> Hedonism -> Achievement -> Power:

dominance -> Power: resources -> Face

-> Security: personal -> Security:

societal -> Tradition -> Conformity:

rules -> Conformity: interpersonal ->

Humility -> Benevolence: dependability

-> Benevolence: caring -> Universalism:

concern -> Universalism: nature ->

Universalism: tolerance.

- Nearby labels on the circle usually express compatible motivations.

- Labels on the opposite side of the circle usually express motivational conflict.

- Multi-label outputs are allowed, especially for nearby or conceptually compatible values.

- Avoid predicting distant/opposing

values together unless the sentence clearly expresses both.

Output rules:

- Return exactly one JSON object with this schema: {"labels": ["Label name", "..."]}

- Use only exact labels from the allowed list. Do not invent labels.

- If no listed value is expressed, return {"labels": []}.

- Do not include explanations, markdown, comments, or text outside the JSON object.

Target sentence:

[sentence] (the target sentence is substituted here)

Sentence (abridged)	Gold	Thresholding	+ Schwartz decoder	F1
<i>...fake advertisements and websites are designed with elements such as discounts and vacation opportunities that consumers tend to be easily persuaded...</i>	Security: societal; Conformity: rules	Security: personal	Security: personal; Security: societal; Conformity: rules	0.00 → 0.80
<i>He stressed that the countries of the region should eventually join the EU, of course within the framework of conditionality...</i>	Conformity: interpersonal	Self-direction: action; Conformity: rules	Conformity: rules; Conformity: interpersonal	0.00 → 0.67
<i>While in the field of regulatory reform it is possible to mark the progress of the parties towards a compromise, when it comes to raising the retirement age for women...</i>	Power: dominance	Power: dominance; Benevolence: dependability; Universalism: concern	Power: dominance	0.50 → 1.00
<i>Provided, however, that the allied countries "remain united in maintaining and increasing sanctions pressure."</i>	Power: resources	Power: dominance	Power: dominance; Power: resources	0.00 → 0.67

Table 9: Representative decoder edits on the test set, drawn from individual seed runs. The first two rows complete nearby true values (the second also removes an opposite-side false positive); the last two remove opposite-side false positives or complete an adjacent value, matching the two examples discussed in Section 7. F1 is the sentence-level F1 before → after decoding.